ADVANCED THERMAL MANAGEMENT STRATEGY FOR ARC-BASED DIRECTED ENERGY DEPOSITION ASSISTED BY NUMERICAL MODELING

T. REINDL*, N. HEMPEL*, P. MAYR*

**Technical University of Munich, TUM School of Engineering and Design, Chair of Materials Engineering of Additive Manufacturing, 85748 Garching, Germany, 0009-0008-4786-8428, 0000-0001-7316-1065, 0000-0003-2530-4644,*
th.reindl@tum.de *(corresponding author)*, nico.hempel@tum.de, peter.mayr@tum.de

DOI 10.3217/978-3-99161-089-2-013, license CC BY 4.0

ABSTRACT

Arc-based Directed Energy Deposition (DED-Arc) offers major industrial potential due to its versatile application possibilities and attractive advantages, such as the flexible, time-efficient near-net-shape manufacturing of large-volume components. However, there are obstacles to overcome, such as the complex thermal history, which limits process stability, component quality, and process efficiency. Therefore, establishing this technology in industry requires solutions capable of monitoring and managing temperature fields. In this context, the focus is increasingly shifting toward real-time-capable, physically based digital solution frameworks. Current efforts primarily emphasize monitoring, simulation, or trial-and-error methods. There is a lack of direct coupling between energy-temperature metrics, standardized analyses and classifications, and effective process optimizations, including adaptive control strategies and design foundations for advanced thermal management.

This work aims to strategically analyze and classify the coupled data from an industrial-grade digital shadow (DS) and numerical modeling. Based on this, targeted optimization measures and process control indicators are identified to enable advanced thermal management. To achieve this, a novel thermal optimization strategy (TOS) was developed to optimize the thermal process of an exemplary tube geometry. Optimizations in path planning, interlayer temperature (ILT) profiles, and temperature change rates were detected and addressed with specific countermeasures. An analysis of the heat balance revealed specific temperature and heat flow gradients providing input for targeted cooling actions. The results highlight the benefits of a coupled monitoring-simulation-control architecture, which eliminates process errors early, enhances thermal stability and control, and optimizes process efficiency.

Keywords: Digital Shadow, Digital Twin, Directed Energy Deposition, Numerical Modeling, Process Optimization, Thermal Management, Thermal Optimization Strategy

INTRODUCTION

Additive manufacturing (AM) is gaining increasing attention as a valuable technology that complements traditional manufacturing methods. This trend is reinforced by the industry exploring its potential for a wide range of applications and pushing its boundaries. These factors also drive interest in arc-based Directed Energy Deposition (DED-Arc), which offers attractive benefits such as near-net-shape manufacturing of large-volume complex components with high deposition rates [1,2]. This AM process also opens up new possibilities, such as multi-material manufacturing and repair applications [1,3]. Despite the promising technological advantages and possibilities, some challenges must be tackled before DED-Arc becomes further industrially established.

One major issue is the lack of understanding and targeted control of thermal behavior during the process. Poor heat control can cause significant process inefficiencies and deteriorated component properties, ranging from residual stresses and insufficient geometric accuracy to inhomogeneities in the microstructure [2,4-6]. However, thermal profiles and phenomena are difficult to predict, monitor, and control accurately due to the inherent complexity of heat transfer and its effects on the material [5,6]. Addressing this challenge requires a holistic approach that combines multiple research areas. The primary objective is to digitally map and simulate the DED-Arc process and optimize heat transfer in terms of process efficiency and component quality.

Numerical modeling is a key methodology for predicting and analyzing AM processes in depth [7]. As shown in the review by Sampaio et al. [8], DED-Arc simulations can be divided into macro, meso, and micro simulations based on the level of detail. Macro approaches are frequently used for thermal investigations. For example, Farias et al. [9] showed that macro simulations using Simufact Welding software can help predict the resulting interlayer temperatures (ILT) for varying idle times in conjunction with an artificial neural network. Zamiela et al. [10] demonstrated an approach in which the simulation is combined with in situ thermal data to generate a comprehensive thermal history, which is further used for surface deformation detection. Numerical analysis by Hackenhaar et al. [11] using LS-DYNA proved that air jet impingement can significantly influence and control the ILT. Fast simulation methods for thermal management of thin-walled structures [12] or temperature and phase transitions [13] have even used 2D approaches with some simplifications, maintaining high accuracy. This shows that achieving sufficient accuracy quickly and with minimal effort is crucial.

Monitoring is also essential for DED because it can capture the thermal history and numerous other process variables, enabling defect detection and targeted process intervention. Various multi-sensor approaches and frameworks have been developed, providing a digital shadow (DS) [14,15] of the process or even leading to a digital twin (DT) [16-19]. Primarily, process parameters directly related to the energy input (e.g., current, voltage, laser power, robot speed) or the deposition rate (e.g., wire feed rate, powder feed rate) were varied as control variables. This is usually insufficient to fully control the thermal history, because regulating the energy input only works at the deposition spot and is limited to natural cooling rates when the process is paused. Further developments are still needed for an energy- and time-optimized temperature-controlled process.

Together with process prediction and monitoring, the process control strategy and the implementation of thermal management are crucial. Nagallapati et al. [20] distinguished between passive and active management approaches and demonstrated significant influences on mechanical component properties, distortion, and residual stresses. Reis and Da Silva [21] classified thermal management even more precisely into intrinsic, active, passive, and natural types. Intrinsic methods adjust process parameters in response to local heat input (cf. [22,23]), while passive management modifies heat conduction through substrate adjustments, such as water cooling (cf. [24-26]). Active methods, such as near-immersion active cooling (NIAC), significantly reduce component temperatures and process times (cf. [25,27,28]). Other flexible techniques utilize targeted fluid streams to enhance cooling rates and influence the mechanical properties (cf. [26,29]). Natural methods involve process interruptions and surrounding effects. However, much research is generally based on trial and error, without focusing on the precise and targeted use of these techniques, leaving the potential of many thermal management approaches unfulfilled.

This work aims to methodically analyze and classify both measured data and model-based data and predictions to implement targeted thermal process optimization and control within the context of advanced thermal management. For this purpose, a potentially real-time-capable strategy for evaluating and classifying thermal behavior during production must be developed, maximizing component quality and thermal stability while balancing energy and process efficiency through appropriate control measures. Numerical models are created in Simufact Welding and validated using measured data from a DS and metallographic cross-section analyses to achieve these goals. The captured temperature data are strategically processed with MATLAB to derive classified control and optimization data that can be fed directly into the process and the simulation for further iterations. Furthermore, specific design requirements and limitations are derived for required temperature-influencing external elements, like heating or cooling units. The strategy is then critically evaluated regarding industrial applicability and potential real-time capability with extension to a DT.

METHODOLOGY

The methodological basis of this work comprises five different interrelated key modules, as shown in Fig. 1. A core element is the so-called Thermal Optimization Strategy (TOS), which combines the last three stages of the visualized methodology. Starting from the DED-Arc process, a DS is generated based on time-synchronized measurement data, and an additional validated numerical model is set up. This enables precise process monitoring and process prediction. The numerically and metrologically obtained data further serve as input for thermo-energetic analyses and classifications. Based on component and process requirements, optimization steps are derived and, if necessary, iterated again using numerical modeling. The resulting optimizations are implemented ex situ or, in the case of a real-time process chain, in situ with bidirectional communication as part of a DT framework.

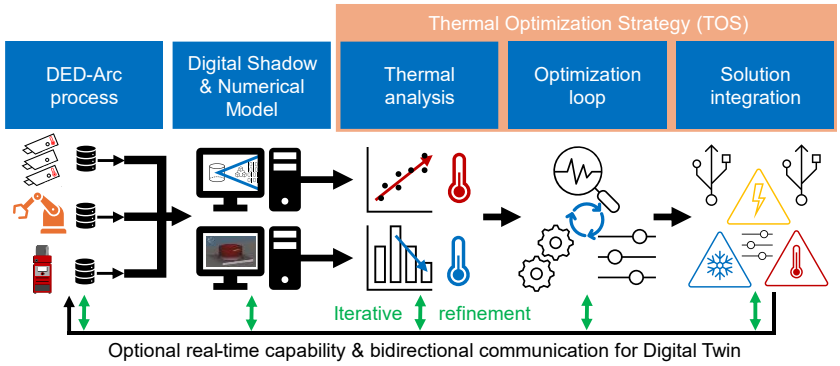

Fig. 1 Schematic representation of the workflow and methodology

The process sequence involves gas metal arc welding (GMAW) as a wire-based DED-Arc technology, using a Fronius TPS 400i welding power source operated by a six-axis KUKA KR 70 R2100 industrial robot. An advanced version of the framework described in [15] generates the DS. This includes process data from the welding source (gas flow, welding current, voltage, wire feed rate, arc stability), position data from the torch, thermal measurements using thermocouples (type K), pyrometers (Optris CT series, measuring ranges: 50-400 °C or 200-1500 °C), and a thermal imaging camera (Optris Xi400, measuring ranges: 150-900 °C or 200-1500 °C), as well as melt pool, layer geometry, and stick-out monitoring (Cavitar C300 welding camera). The applied framework is illustrated in Fig. 2.

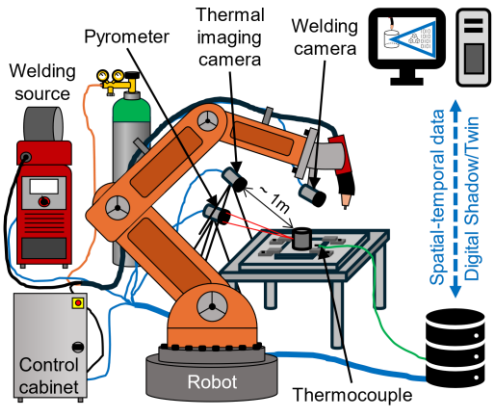

Fig. 2 Schematic of experimental setup

A supplementary numerical model derived from the high-precision data from the DS provides even more detailed temperature data and potential for prediction. Based on the spatial-temporal geometry and welding source data, a simplified component geometry is created using the double-ellipsoid heat source model, as described by Goldak [30]. The

measured thermal data is used for further model calibration and accuracy improvement. The time efficiency of this approach is enhanced using a macro simulation as classified in [8], which can be performed either thermally or thermo-mechanically. This modeling enables precise measurement and analysis of temperature profiles throughout the process, even in hidden measurement areas. Similar to [9,24,31], the commercial simulation software Simufact Welding is utilized in this work.

The thermal data from the DS and the simulation are implemented in the three-stage TOS. The three stages - thermal analysis, optimization loop, and solution integration - involve four key areas of action. These are divided into energy input, temperature profile, rate of temperature change, and heat control, ranging from path planning to post-weld heat treatment. Fig. 3 provides a comprehensive overview of the TOS scheme.

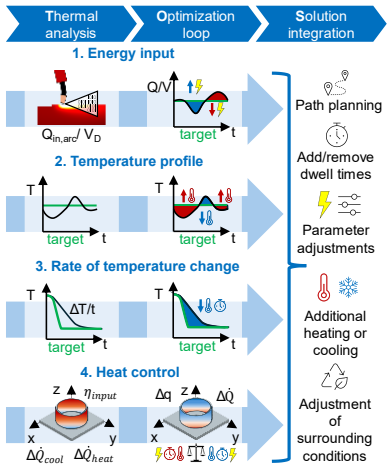

Fig. 3 Workflow of the TOS procedure

The first area of action, energy input, considers the energy per unit length E_L based on the welding current I, welding voltage U, and travel speed v at a certain efficiency η, and classifies it according to the deposited target volume $V_{D,target}$. This volume is calculated in a simplified manner, depending on the wire cross-sectional area and the wire feed speed v_w during a defined time interval t. The volumetric energy density VED is then calculated from the energy input by the welding source $Q_{in,arc}$ per V_D, and is also considered incrementally and cumulatively. The equations are therefore composed as follows:

$$E_L(t) = \frac{\eta(t) \cdot U(t) \cdot I(t)}{v(t)} \tag{1}$$

$$V_D(t) = \frac{d_w^2 \cdot \pi \cdot v_w(t)}{4} \cdot t \tag{2}$$

$$VED^{[t_0,t_1]} = \frac{Q_{in,arc}}{V_D} = \frac{\int_{t_0}^{t_1} \eta(t) \cdot U(t) \cdot I(t)\, dt}{\int_{t_0}^{t_1} \dot{V}_D(t)\, dt} \tag{3}$$

The MATLAB script analyzes spatial-temporal data based on Eq. (3) to identify correlations between energy peaks and geometric features or process irregularities. The time-interval and location-correlated *VED* values are set in relation to the idealized VED_{target} values as VED/VED_{target}. In addition, the ratios $Q_{in,arc}/Q_{in,arc,target}$ and $V_D/V_{D,target}$ are evaluated. Based on the percentage deviations, a classification is made into undercooled/over-deposited, overheated/under-deposited, and tolerated target zones. Afterwards, optimization is carried out, leading to a variation in the welding parameters, motion sequence, or even modified path planning. Using external heating or cooling sources is also an option. It is crucial to consider the relations of the three ratios to correctly interpret and remedy the thermal discrepancies.

The temperature profiles and the rates of temperature change (second and third areas of action) are analyzed at defined measuring points or intervals, with a distinction made between stationary (e.g., seam location) and moving measuring methods (e.g., relative position to the moving torch). Based on a MATLAB script, time-resolved deviations between actual and target temperatures are localized and classified again into tolerated, undercooled, and overheated zones. Predefined material or component-specific intolerable extreme values are identified and flagged accordingly. The combined classification enables the iterative numerical determination of specific optimization approaches, such as targeted process interventions or additional cooling and heating sources, based on the recorded location-time data.

The fourth area of action is heat control, which focuses on the energy balance of the DED-Arc process and final approaches for targeted and potential real-time thermal management. This involves analyzing the energy input via the arc $Q_{in,arc}$, additional heating elements or phenomena $Q_{in,other}$, and losses due to convection Q_{conv}, radiation Q_{rad}, conduction Q_{cond}, and additional cooling elements and phenomena $Q_{out,other}$, all correlated with the process time. The simplified equation for the thermal equilibrium, including the change in internal energy ΔU_i, can be expressed as:

$$Q_{in,arc}(t) + Q_{in,other}(t) = \Delta U_i(t) + Q_{conv}(t) + Q_{rad}(t) + Q_{cond}(t) + Q_{out,other}(t) \quad (4)$$

The equations for the associated internal energy and the heat transfer rates are given in the following, including surface and contact areas (A_s and A_c), component volume V, Stefan-Boltzmann constant σ, temperature-dependent density values ρ, convective heat transfer coefficient h, contact conductivity coefficient h_c, specific heat capacity c_p, emissivity ε, and location- and time-dependent temperature values (reference T_{ref}, surface T_s, ambient T_∞, substrate T_{sub}, contact T_c):

$$\Delta U_i(t) = \int_V \rho\,(T(x,t)) \left[\int_{T_{ref}}^{T(x,t)} c_p(x,\theta)d\theta\right] dV \quad (5)$$

$$\dot{Q}_{conv}(t) = \int_{A_s} h(T(x,t))[T_s(x,t) - T_\infty(x,t)]dA \quad (6)$$

$$\dot{Q}_{rad}(t) = \int_{A_s} \varepsilon(T(x,t))\sigma[T_s^4(x,t) - T_\infty^4(x,t)]F_{s\to\infty}(x,t)dA \quad (7)$$

$$\dot{Q}_{cond}(t) = \int_{A_c} h_c\big(T(x,t)\big)[T_{sub}(x,t) - T_c(x,t)]dA \quad (8)$$

Based on this, MATLAB is used to classify globally and locally at which moment in the process and to what extent predefined threshold values for energy input or loss are exceeded or undercut. Additionally, temperature variations ΔT and changes in heat flux Δq within the component are identified and predicted. Relating the measured energy fractions to the ideal energy fractions further provides a simplified estimate of the efficiency of the energy input η_{input}, as shown in Eq. (9).

$$\eta_{input} = 1 - \frac{\int_{t_0}^{t}(\dot{Q}_{conv}(\tau)+\dot{Q}_{rad}(\tau)+\dot{Q}_{cond}(\tau)+\dot{Q}_{other}(\tau))d\tau}{\int_{t_0}^{t}(P_{arc,ideal}(\tau)+P_{add,ideal}(\tau))d\tau} \tag{9}$$

Time- and location-specific energy-efficient gradient-controlled heat treatments can also be carried out based on the analysis and classification of the heat balance. $\dot{Q}_{heat}$ and $\dot{Q}_{cool}$ can be estimated as follows:

$$\dot{Q}_{heat}(t) = \frac{1}{\Delta t}\int_V \rho\,(T(x,t))c_p(T(x,t))[T_{target} - T(x,t)]_+ dV \tag{10}$$

$$\dot{Q}_{cool}(t) = \frac{1}{\Delta t}\int_V \rho\,(T(x,t))c_p(T(x,t))[T(x,t) - T_{target}]_+ dV \tag{11}$$

For optimization, it is possible to identify parameters and process conditions that maximize efficiency while monitoring energy losses or accounting for them specifically in thermal process control. Additionally, the targeted energy distribution within the component can be controlled by establishing precise local- or time-graded heating and cooling strategies. This can increase process stability and energy efficiency while minimizing the risk of thermally induced defects. An estimate of the required energy demand for optimizing process time can also be provided.

The final stage in TOS is solution integration. It is essential that the individually derived optimization measures for energy balance and temperature control complement each other harmoniously and do not cancel each other out. While path planning modifications should be made pre-procedurally, parameter variations and adjustments can be made at any time. External cooling and heating solutions can be developed and implemented according to the maximum power levels and gradients that have been investigated. Cooling can be achieved using different fluids and varying flow rates. Heating can be predefined or controlled in situ using different inductors, laser beams, or infrared lights. The additional use of a proportional-integral-derivative (PID) controller can achieve further situational flexibility.

NUMERICAL MODEL AND VALIDATION

To enhance the precision and predictive capabilities of the DS, initial tests are first conducted to set up and validate a numerical model. For this purpose, a tube geometry ($\emptyset_m$ = 100 mm, h = 77 mm) was deposited via controlled/regulated short-arc with reversing wire on a substrate plate (S235) using the standard G3Si1 filler wire ($\emptyset$ = 1.2 mm). A wire feed speed of 2.5 m/min was used, along with a robot movement speed of approximately 0.6 m/min and a defined layer height of 1.1 mm. An 8% CO_2 in Ar shielding gas with a flow rate of ~12 l/min was used. Emissivity coefficients ε in the range of 0.70-0.92 were used for the temperature

measurements for mainly uniformly oxidized surfaces, comparable to the values determined by [32] in the range of 0.70-0.95 for similar conditions and steels.

The numerical model was set up as a transient thermal finite element analysis (FEA) to map the time-dependent thermal process. This included the tube geometry, the substrate, and the base plate. Implementing the clamping tools was neglected due to the punctual clamping mechanism, and was realized as fixed points at identical locations. The multi-phase material models GS1 (deposited material) and S235, included in Simufact Welding (version 2023.4), were used for the simulation, allowing a later extension to a precise thermo-mechanical model. A no-slip condition and a "glued at peak temperature" condition were imposed between the individual simulation components. The contact heat transfer coefficient was defined as 2000 W/m^{2}K, the emission coefficient as 0.8, and the ambient temperature as 20 °C.

The mesh was created using hexahedral elements (Hex8) with a linear interpolation approach, whereby each element has eight nodes and eight integration points. A fine mesh (element size ~1 x 1 x 0.55; 168,000 elements) was applied to the tube to represent the process in detail, and a coarser mesh (element size ~1 x 1 x 1.1; 84,000 elements) was implemented for time-efficient predictions. For precise, high-resolution modeling of the penetration zone and, consequently, the heat transfer area to the substrate, local mesh refinement with a scaling factor of n = 1.2 was performed. The number of adapted elements corresponds to the number of initial elements multiplied by eight to the power of the scaling factor. The Domain Decomposition Method (DDM) and Shared Memory Parallelization (SMP) were employed to reduce the computation time. The simulation was performed using the MUMPS parallel direct solver. A comparison of the high-resolution simulation and the fabricated component is provided in Fig. 4.

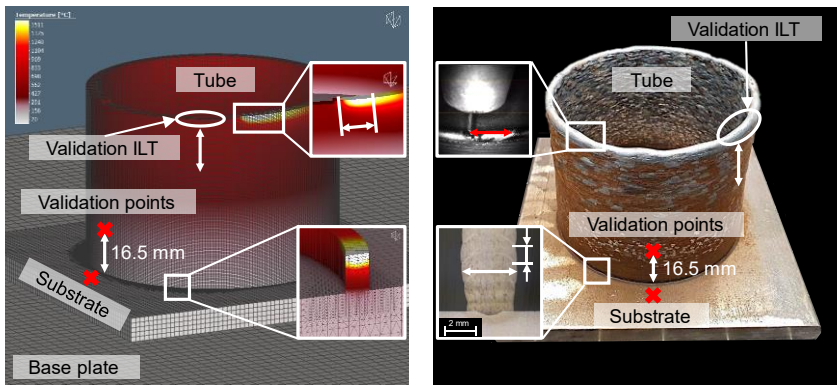

Fig. 4 Numerical model (fine mesh) and component with highlighted validation methods

The heat input from the DED-Arc process was modeled in the simulation using the double-ellipsoid model developed by Goldak. Based on the explanations from Goldak et al. [30], the power density distribution in the front quadrant (Eq. (12)) differs from that in the rear quadrant (Eq. (13)). The sum of the front and the rear fraction (f_f and f_r) equals two, as shown in Eq. (14). $Q_{in,arc}$ is the product of the efficiency of the heat source η, the welding current I, and

the welding voltage *U*. Fig. 5 shows a visualization of the double-ellipsoid heat source model according to Goldak, along with an overview of the parameters used in the present simulation.

$$q_f(x,y,z) = \frac{6\sqrt{3}f_f Q_{arc}}{a_f bc\pi\sqrt{\pi}} \exp(\frac{-3x^2}{b^2})\exp(\frac{-3y^2}{a_f^2})\exp(\frac{-3z^2}{c^2}) \quad (12)$$

$$q_r(x,y,z) = \frac{6\sqrt{3}f_r Q_{arc}}{a_r bc\pi\sqrt{\pi}} \exp(\frac{-3x^2}{b^2})\exp(\frac{-3y^2}{a_r^2})\exp(\frac{-3z^2}{c^2}) \quad (13)$$

$$f_f + f_r = 2 \text{ , with } f_f = \frac{2a_f}{a_f+a_r} \text{ and } f_r = \frac{2a_r}{a_f+a_r} \quad (14)$$

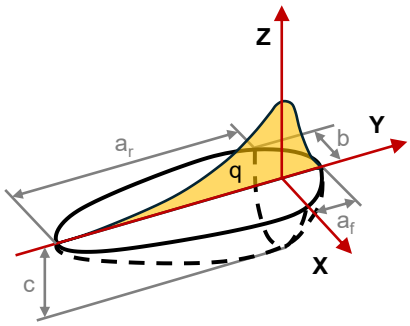

Parameter	Value in mm
a_f	1.8
a_r	7.2
b	2.0
c	3.7

Fig. 5 Double-ellipsoid heat source model according to [30], including the parameter values used in the present simulation

The numerical model was calibrated using the measured temperature fields from the tube deposition test. Selected heat source parameters from Eqs. (12)-(14) and relevant material interaction properties were iteratively adjusted within physically justified limits until the simulated and measured thermal histories aligned. All calibrated values remained constant throughout the simulation. Correlated with the experimental welding parameters, an average E_L of ~1.3 kJ/cm was applied in the simulation. Additionally, the heat source underwent iterative calibration, resulting in a time step width of 0.15 s. Afterwards, the four different approaches visualized in Fig. 4 were used to validate the numerical model. These included fixed-point temperature measurements in Layer 15, ILT, and substrate temperature measurements, investigations of melt pool length, and comparisons of the actual component geometry with the idealized geometry using a cross-section sample.

A comparison of the measured and simulated temperature cycles in the 15th layer is shown in Fig. 6. The minor deviations between the pyrometer and thermal imaging camera measurements demonstrate the reliability of the measurement method. The simulation with a fine mesh revealed temperature deviations of less than 50 °C for the critical extreme values near the heat source, confirming the validity of the numerical model. A coarser mesh resulted in deviations at the peak temperatures, mainly in the range of 50-100 °C. Despite these fluctuations, the heating and cooling curves correspond very well, with only minor differences of a few degrees Celsius. Although the discrepancies limit the applicability for detailed

numerical process replication, the coarser modeling shows excellent potential as a computationally efficient alternative for fast process prediction.

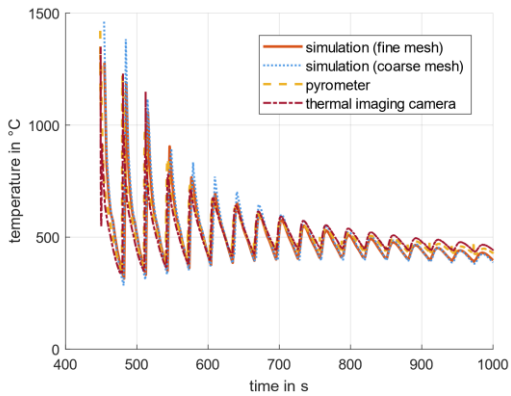

Fig. 6 Fixed-point measurement validation in Layer 15

The determined substrate temperature profiles and the ILT curves are shown in Fig. 7. The deviations between the measured and simulated substrate plate temperatures were below 50 °C for the detailed model. In contrast, for the coarse model, the differences remained below 70 °C. In general, there were obvious discrepancies between the simulation and the experiment, attributable to the fact that distortion was not considered in the simulation. Consequently, the contact conditions were idealized. The simulated ILT curves showed good agreement with the experiment. As the measurements were taken simultaneously for each layer, comparisons can also be made using the root mean square error (RMSE). The value for the coarse mesh is RMSE = 12.7 °C, while the fine mesh achieved RMSE = 9.7 °C (~25% lower). The validity of the precise simulation is proven once again, as is the ability of the coarse simulation to provide sufficiently accurate predictions.

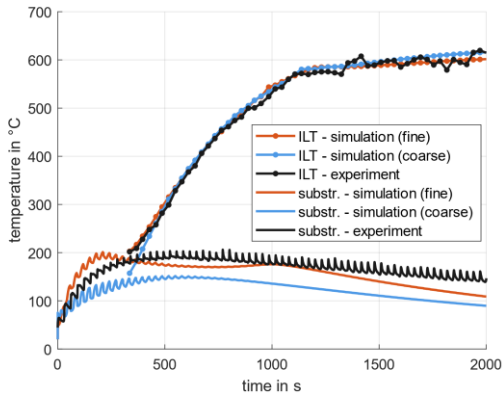

Fig. 7 Comparison of ILT and substrate temperature measurements

The geometric analysis of the tube geometry of the experiment (cf. Table 1) indicates that suitable geometric simplifications were applied, resulting in deviations of $\leq 5\%$. The experimentally obtained melt pool length varied from 6.5 to 15.8 mm. By comparison, the detailed simulation yielded an RMSE of 0.64 mm, while the coarse simulation resulted in an RMSE of 0.94 mm (~47% higher). Since the simulation does not include dynamic melt pool motions and fluid simulations, both values are within a sufficiently accurate range, ensuring the validity of the numerical models.

Table 1 Geometrical and melt pool data

	Experiment	Simulation
Mean layer width in mm	3.8 ± 0.2	4.0
Mean layer height in mm	1.1 ± 0.1	1.1
Mean total height in mm	77.5 ± 0.1	77.0
Melt pool length in mm	range: 6.5-15.8	RMSE = 0.64 (fine mesh) RMSE = 0.94 (coarse mesh)

RESULTS

The data from the DS and the validated numerical model of the tube geometry are used to further verify and demonstrate the applicability and output of TOS. As targeted thermal management of the DED-Arc process is very versatile and application-specific, the focus was placed on representative standard challenges and applications. For this purpose, the four areas of action of TOS were executed to identify and demonstrate optimization approaches and an advanced control strategy.

The first area, energy input, involved analyzing the torch movements based on the axis movements of the robot in correlation with the welding source parameters. This revealed that movements in the X and Y directions were repeatedly interrupted for 0.3 s at the seam, while the stick-out was readjusted according to the layer height in the Z direction. Fig. 8 shows representative data for the seam transition from the first to the second layer, where the coordinate origin is located at the center of the tube on the substrate surface. The analysis of the ratios of measured values to target values, based on 1-second intervals, yielded $VED = VED_{target}$ for the volumetric energy density, indicating a stable process. The correlating ratios $V_D/V_{D,target}$ and $Q_{in,arc}/Q_{in,arc,target}$ (ratios = 1.3) indicate a material and energy surplus of 30%, which was attributable to the short process delay. This significantly classified irregularity implies a systematic error in the path planning, which led to measurable geometric deviations and temperature peaks. As an optimization for follow-up investigations, the Z movement at the seam was performed as a ramp over several seconds with continuous movement in the X-Y direction. The remaining error is within the tolerance range. Additionally, a total process time saving of ~21 s was achieved.

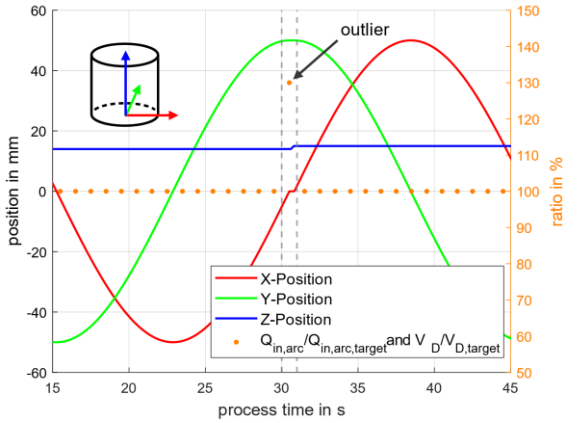

Fig. 8 Energy input analysis at the tube seam

The second area of action involved analyzing the ILT profile of the manufactured tube. As shown in Fig. 9, the classification into the three zones, overheated, undercooled, and tolerated (200 ± 10 °C; 5% deviation), was conducted concerning the target ILT of 200 °C. The undercooled zone could be easily eliminated by using substrate preheating/heating. The overheated zone is a more complex case, so this study focused on the simplified criterion of ILT ≤ 200 °C, allowing the undercooled zone to remain unchanged. Process interruptions were introduced as an energy-efficient but highly time-consuming optimization strategy, whereby the next layer was only deposited once the criterion ILT ≤ 200 °C was met. As a result, no additional cooling elements were required.

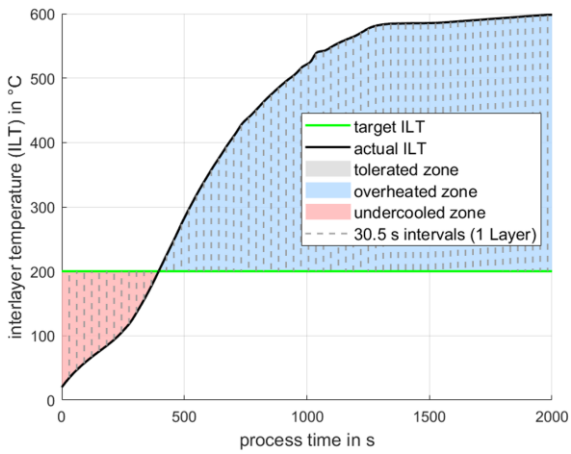

Fig. 9 Analysis and classification of ILT profiles

The calculated predictions for tube manufacturing with process interruptions to maintain ILT showed an increase in total process time by a factor of 2.8, reaching almost 1 hour and 40 minutes. This timely inefficiency led to the third area of action of TOS, which addressed the rate of temperature change over time. As shown in Fig. 10 for layer 50, the target cooling phase was compared with the predicted cooling phase and classified. Only the overheated zone could be identified, as only increased cooling is required. Overall, the cooling time from deposition to the target temperature of 200 °C should occur within 30.5 s for a non-stop process. In this case, the cooling cycle to 200 °C must be reduced by ~55 s. There are various ways of improvement, ranging from a cooling sequence that is as natural as possible, as in the example, to optimization with the lowest possible cooling capacity required. Based on the classification, the required cooling capacity for each time interval and location can be derived for process design and thermal management planning. In addition, it would be possible to influence the material properties in a targeted manner by controlling the t8/5 cooling rates (from 800 to 500 °C). Nevertheless, these calculations and approaches must be carried out according to individual circumstances and cooling options. However, all data required for strategic thermal management can be obtained from this analysis and classification.

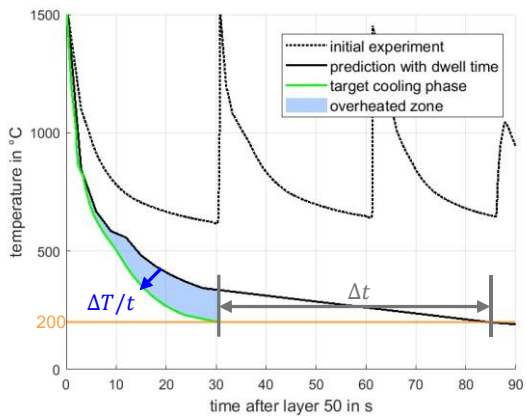

Fig. 10 Analysis and classification of rates of temperature change

The final area of action involves analyzing the overall thermal condition of the component. Besides recording and classifying heat losses, heat input, and efficiency factors, the primary focus within this study is on the relevant temperature fields and heat flux gradients. Fig. 11 shows a component section classified using heat maps. The temperature distribution is shown on the left, and the heat flux distribution is shown on the right. The simulated dataset, based on real experimental conditions, is visualized at the top, and the predicted solution with implemented dwell phases to comply with the ILT condition (≤ 200 °C) is shown at the bottom. The temperature differences varying across the surface can be determined by comparing the temperature fields at the defined component position. The classification clearly shows the component height at which significant cooling is required to maintain the sample profile with the cooling times. A comparison of the heat flux data shows that maintaining the

ILT reduces the thermal changes and variations, which in turn influence fewer previous layers significantly. In addition, fluctuations in Δq in the circumferential direction are also visible.

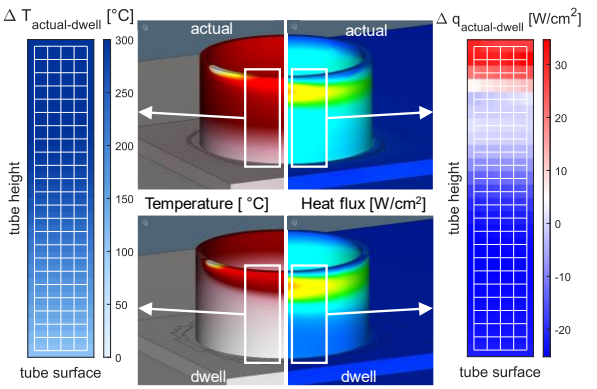

Fig. 11 Analysis and classification of ΔT and Δq for location-specific heat control

The data processed using TOS shows the cooling and heating actions required for each component area to achieve targeted thermal management. This final optimization step enables the precise implementation of specific process interventions in real-time, such as adjusting the welding source or robot parameters, or interrupting and resuming processes, while maintaining time and energy efficiency. The targeted additional control of external cooling and heating elements is more complex. However, it has been shown that temperature-specific influences can promote and specifically create homogeneous temperature fields. Based on this, design recommendations and requirements for cooling and heating units can be derived, which can then even be controlled via the output values of the DS to achieve an even more advanced thermal process management.

The computation times highlight the overall efficiency and current limitations of the framework. Data acquisition and thermal analysis run within seconds up to near real-time, depending on data volume and complexity. In contrast, numerical model predictions still require several hours, depending on mesh resolution and geometry, with optimization and solution integration times similarly scaling with complexity. These results illustrate both the current capabilities and the remaining potential for further improvement.

DISCUSSION

The results demonstrated the effectiveness of the data framework, coupled with TOS, in precisely analyzing energy and material inputs, temperature profiles, rates of temperature change, and heat flows for a DED-Arc process. This foundation enables the validation of existing process parameters and serves as a basis for developing thermally optimized control and process management strategies that directly impact component quality and process efficiency. However, for standard industrial implementation and further development, several

issues must be critically examined, ranging from real-time capability and system accuracy to process efficiency.

The study demonstrated that thermal conditions can be recorded and fed back in real-time with practical latency using the advanced framework developed by [15]. However, one major challenge in real-time recording of thermal data in DED-Arc is the varying emission factor, which can vary greatly depending on material, temperature, and surface properties, as the studies [31-33] demonstrate. This can be remedied by applying a corrective overlay to the measurement data or using supporting, fast simulations, as described in [13]. As the review papers [18,19] indicate, it is important to use automated rule-based decision models. TOS provides an initial foundation for this, considering that certain optimization steps can be performed offline before or after the process. According to [18], it is also important to focus only on the real-time control of relevant process parameters to keep computing time and the required computing power of the DT within realistic limits.

Another critical factor in data acquisition, automated analysis, and automated classification for achieving advanced thermal management supported by TOS is the volume of data and the need for efficient processing. This will necessitate robust machine learning (ML) pipelines or the integration of advanced artificial intelligence (AI) for an industrial solution, as suggested by [15]. Furthermore, physics-informed neuronal networks (PINN) can accelerate the prediction of temperature fields compared to FEA and enable precise online parameter identification, as demonstrated by [34,35]. Another work from Mattera and Nele [36] demonstrated real-time ML-based anomaly/defect detection from process signals. Consequently, these studies highlight how real-time and automated TOS implementation for advanced thermal management could be achieved despite high data volumes from DS, simulation, or DT. However, the existing framework needs further development, for example, with targeted ML or PINN approaches to achieve this.

The review by Reis and Da Silva [21] shows that thermal management can be implemented with varying degrees of complexity, flexibility, and efficiency. Their outlook also highlights the need to take a broader, critical view of the additional costs that arise and the balance between the required effort and the process efficiency achieved through the management strategies. In this context, TOS combined with the presented framework is a suitable solution, as the optimization options for targeted thermal management can be precisely defined according to the present possibilities. This can range from offline adjustment of the welding parameters to a DT solution with in situ temperature control by external heat elements. An important aspect is that the final area of action of TOS involves a comprehensive thermal and energy balance of the process, which can also result in additional costs due to energy expenses or downtimes, or cost savings due to quality improvements and reduced process times. This enables component-specific design based on economic preferences and technical feasibility, leading to advanced thermal management.

SUMMARY & OUTLOOK

The study demonstrated the successful application of the newly developed TOS and the data generation to achieve advanced thermal management on an example tube geometry. To this

end, a data acquisition framework was expanded to include measured thermal and process data as a DS. Additionally, numerical modeling using FEA was established, which was validated for detailed process representation and prediction. By systematically linking these data, all three stages (thermal analysis, optimization loop, and solution integration), including the four areas of action of TOS (energy input, temperature profile, rate of temperature change, and heat control), were carried out for standard challenges and applications in DED-Arc using the exemplary component. The available data, fundamental modules of an advanced thermal management system, were analyzed and strategically classified. Individual optimization potential and options were derived based on thermodynamic basics. Considering economic and financial circumstances, this provided a clear foundation for decision-making in designing an idealized thermal process management system for individual use cases. The key findings can be summarized as follows:

- An industrial-grade DS framework was extended with validated thermal numerical models to enable advanced process monitoring, replication, and prediction.
- An innovative TOS was created that systematically summarizes, analyzes, and classifies all gained data and allows for identifying optimization opportunities that can take thermal requirements, influences on process complexity, and economic factors into account.
- Using the tube sample, a robot path error that previously caused energy and material surpluses was eliminated using fundamental control equations. Moreover, the ILT could be specifically controlled to prevent overheating.
- Further iterative simulations allow for precise time- and location-dependent derivation of necessary cooling or heating actions to optimize the efficiency of the process, depending on component specifications and process capabilities.
- The heat flow analysis demonstrated the significant influence of ILT control and the associated impact on the thermal balance, from which adaptive cooling/heating with maximum energy efficiency can be derived and used for closed-loop control.

The discussion critically examined the TOS and general thermal management for DED-Arc, focusing primarily on real-time capability, data processing, and the balance between industrial applicability and the associated costs with increasing process complexity. The existing framework, in conjunction with the TOS, offers innovative solutions to significant temperature-related process challenges. However, further improvements are required, particularly in the areas of rapid automated data management and process control. Consequently, the following future steps were identified:

- Implement the proposed heat control logic in a real-time feedback system with closed-loop control.
- Use the generated large amounts of thermal and process data for AI-supported optimization loops.
- Further apply TOS to complex, industry-oriented geometries for validation and demonstration of scalability.
- Extend it with thermo-mechanical considerations to realize specific mechanical component properties by using TOS.

- Upgrade to a fully real-time-capable DT framework, where TOS is integrated as an automated decision logic and in situ control foundation.

ACKNOWLEDGEMENT

This project is supported by the Federal Ministry for Economic Affairs and Climate Action (BMWK) on the basis of a decision by the German Bundestag. Furthermore, the support from the project-involved colleagues from Heidenbluth GmbH and Satron Steuerungstechnik GmbH is gratefully acknowledged.

References

[1] D. SVETLIZKY, M. DAS, B. ZHENG, A. L. VYATSKIKH, S. BOSE, A. BANDYOPADHYAY, J. M. SCHOENUNG, E.J. LAVERNIA, N. ELIAZ: 'Directed energy deposition (DED) additive manufacturing: Physical characteristics, defects, challenges and applications', *Materials Today*, 49 (2021), 271-295, https://doi.org/10.1016/j.mattod.2021.03.020.

[2] S. C. COSTELLO, C. R. CUNNINGHAM, F. XU, A. SHOKRANI, V. DHOKIA, S. T. NEWMAN: 'The state-of-the-art of wire arc directed energy deposition (WA-DED) as an additive manufacturing process for large metallic component manufacture', *International Journal of Computer Integrated Manufacturing*, 36 (2023), 469-510, https://doi.org/10.1080/0951192X.2022.2162597.

[3] A. HAKAMI, S. A. OJO, D. V. ABERE, F. D. UZUH, R. A. ROBERT: 'Advancements in metal additive manufacturing: opportunities, limitations, impact on properties, and potential solutions: a review', *Prog. Addit. Manuf.*, 10 (2025), 4447-4495, https://doi.org/10.1007/s40964-024-00885-6.

[4] M. CHATURVEDI, E. SCUTELNICU, C.C. RUSU, L.R. MISTODIE, D. MIHAILESCU, A.V. SUBBIAH: 'Wire Arc Additive Manufacturing: Review on Recent Findings and Challenges in Industrial Applications and Materials Characterization', *Metals*, 11 (2021), 939, https://doi.org/10.3390/met11060939.

[5] L. P. RAUT, R. V. TAIWADE: 'Wire Arc Additive Manufacturing: A Comprehensive Review and Research Directions', J. of Materi. Eng. and Perform., 30 (2021), 4768-4791, https://doi.org/10.1007/s11665-021-05871-5.

[6] N. A. ROSLI, M. R. ALKAHARI, M. F. B. ABDOLLAH, S. MAIDIN, F. R. RAMLI, S. G. HERAWAN: 'Review on effect of heat input for wire arc additive manufacturing process', *Journal of Materials Research and Technology*, 11 (2021), 2127-2145, https://doi.org/10.1016/j.jmrt.2021.02.002.

[7] A. LOVE, O. A. VALDEZ PASTRANA, S. BEHSERESHT, Y. H. PARK: 'Advancing Metal Additive Manufacturing: A Review of Numerical Methods in DED, WAAM, and PBF', *Metrology*, 5 (2025), 30, https://doi.org/10.3390/metrology5020030.

[8] R. SAMPAIO, J. PRAGANA, I. BRAGANÇA, C. SILVA, C.V. NIELSEN, P. MARTINS: 'Modelling of wire-arc additive manufacturing – A review', *Advances in Industrial and Manufacturing Engineering*, 6 (2023), 100121, https://doi.org/10.1016/j.aime.2023.100121.

[9] F. W. C. FARIAS, J. DA CRUZ PAYÃO FILHO, V. H. P. MORAES E OLIVEIRA: 'Prediction of the interpass temperature of a wire arc additive manufactured wall: FEM simulations and artificial neural network', *Additive Manufacturing*, 48 (2021), 102387, https://doi.org/10.1016/j.addma.2021.102387.

[10] C. ZAMIELA, R. STOKES, W. TIAN, H. DOUDE, M. W. PRIDDY, L. BIAN: 'Physics-Informed Approximation of Internal Thermal History for Surface Deformation Predictions in Wire Arc Directed Energy Deposition', *Journal of Manufacturing Science and Engineering*, 146 (2024), 081007, https://doi.org/10.1115/1.4065416.

[11] W. HACKENHAAR, J. A. MAZZAFERRO, F. MONTEVECCHI, G. CAMPATELLI: 'An experimental-numerical study of active cooling in wire arc additive manufacturing', *Journal of Manufacturing Processes*, 52 (2020), 58-65, https://doi.org/10.1016/j.jmapro.2020.01.051.

[12] P. QVALE, E. B. NJAASTAD, T. BRÆIN, X. REN: 'A fast simulation method for thermal management in wire arc additive manufacturing repair of a thin-walled structure', *Int. J. Adv. Manuf. Technol.*, 132 (2024), 1573-1583, https://doi.org/10.1007/s00170-024-13427-9.

[13] D. WEISZ-PATRAULT: 'Fast simulation of temperature and phase transitions in directed energy deposition additive manufacturing', *Additive Manufacturing*, 31 (2020), 100990, https://doi.org/10.1016/j.addma.2019.100990.

[14] H. MU, F. HE, L. YUAN, P. COMMINS, D. DING, Z. PAN: 'A digital shadow approach for enhancing process monitoring in wire arc additive manufacturing using sensor fusion', *Journal of Industrial Information Integration*, 40 (2024), 100609, https://doi.org/10.1016/j.jii.2024.100609.

[15] G. SAFRONOV, H. THEISINGER, V. SAHLBACH, C. BRAUN, A. MOLZER, A. THIES, C. SCHUBA, M. SHIRAZI, T. REINDL, A. HÄNEL, P. ENGELHARDT, S. IHLENFELDT, P. MAYR: 'Data Acquisition Framework for spatio-temporal analysis of path-based welding applications', *Procedia CIRP*,130 (2024), 1644-1652, https://doi.org/10.1016/j.procir.2024.10.295.

[16] M. M. MAHDI, M. S. BAJESTANI, S. D. NOH, D. B. KIM: 'Digital twin-based architecture for wire arc additive manufacturing using OPC UA', *Robotics and Computer-Integrated Manufacturing*, 94 (2025), 102944, https://doi.org/10.1016/j.rcim.2024.102944.

[17] V. KARKARIA, A. GOECKNER, R. ZHA, J. CHEN, J. ZHANG, Q. ZHU, J. CAO, R.X. GAO, W. CHEN: 'Towards a digital twin framework in additive manufacturing: Machine learning and bayesian optimization for time series process optimization', *Journal of Manufacturing Systems*, 75 (2024), 322-332, https://doi.org/10.1016/j.jmsy.2024.04.023.

[18] H. MU, F. HE, L. YUAN, P. COMMINS, H. WANG, Z. PAN: 'Toward a smart wire arc additive manufacturing system: A review on current developments and a framework of digital twin', *Journal of Manufacturing Systems*, 67 (2023), 174-189, https://doi.org/10.1016/j.jmsy.2023.01.012.

[19] H. LI, X. SHI, B. WU, D. R. CORRADI, Z. PAN, H. LI: 'Wire arc additive manufacturing: A review on digital twinning and visualization process', *Journal of Manufacturing Processes*, 116 (2024), 293-305, https://doi.org/10.1016/j.jmapro.2024.03.001.

[20] V. NAGALLAPATI, V. K. KHARE, A. SHARMA, S. SIMHAMBHATLA: 'Active and Passive Thermal Management in Wire Arc Additive Manufacturing', *Metals*, 13 (2023), 682, https://doi.org/10.3390/met13040682.

[21] R. P. REIS, L. J. DA SILVA: 'Thermal management approaches for arc additive manufacturing: a comprehensive review over a decade of developments and applications', Int. J. Adv. Manuf. Technol., 136 (2025), 1805-1931, https://doi.org/10.1007/s00170-024-14791-2.

[22] F. CHEN, Y. YANG, H. FENG: 'Regional Control and Optimization of Heat Input during CMT by Wire Arc Additive Manufacturing: Modeling and Microstructure Effects', *Materials* (Basel), 14 (2021), https://doi.org/10.3390/ma14051061.

[23] S. SRIVASTAVA, R. K. GARG, A. SACHDEVA, V. S. SHARMA, S. SINGH: 'An Experimental–Numerical Investigation for Layer-Wise-Heat-Input Management in GMA-Based Additive *Manufacturing*', *J. Inst. Eng. India Ser. C*, 103 (2022), 1059-1070, https://doi.org/10.1007/s40032-022-00868-y.

[24] T. REINDL, N. HEMPEL, P. MAYR: 'Effect of substrate preheating and in situ cooling on dimensional accuracy, microstructure, and hardness of wire-arc directed energy deposition components', *Weld World*, (2025), https://doi.org/10.1007/s40194-025-02104-4.

[25] L. J. DA SILVA, D. M. SOUZA, D. B. DE ARAÚJO, R. P. REIS, A. SCOTTI: 'Concept and validation of an active cooling technique to mitigate heat accumulation in WAAM', *Int. J. Adv. Manuf. Technol.*, 107 (2020), 2513-2523, https://doi.org/10.1007/s00170-020-05201-4.

[26] U. REISGEN, R. SHARMA, S. MANN, L. OSTER: 'Increasing the manufacturing efficiency of WAAM by advanced cooling strategies', *Weld World*, 64 (2020), 1409-1416, https://doi.org/10.1007/s40194-020-00930-2.

[27] F. M. SCOTTI, F. R. TEIXEIRA, L. J. DA SILVA, D. B. DE ARAÚJO, R. P. REIS, A. SCOTTI: 'Thermal management in WAAM through the CMT Advanced process and an active cooling technique', *Journal of Manufacturing Processes*, 57 (2020), 23-35, https://doi.org/10.1016/j.jmapro.2020.06.007.

[28] F. R. TEIXEIRA, F. M. SCOTTI, V. L. JORGE, A. SCOTTI: 'Combined effect of the interlayer temperature with travel speed on features of thin wall WAAM under two cooling approaches', *Int. J. Adv. Manuf. Technol.*, 126 (2023), 273-289, https://doi.org/10.1007/s00170-023-11105-w.

[29] C. MA, C. LI, Y. YAN, Y. LIU, X. WU, D. LI, Y. HAN, H. JIN, F. ZHANG: 'Investigation of the in-situ gas cooling of carbon steel during wire and arc additive manufacturing', *Journal of Manufacturing Processes*, 67 (2021), 461-477, https://doi.org/10.1016/j.jmapro.2021.05.022.

[30] J. GOLDAK, A. CHAKRAVARTI, M. BIBBY: 'A new finite element model for welding heat sources, Metall Trans B', 15 (1984), 299-305, https://doi.org/10.1007/BF02667333.

[31] Y. OSAMA, M. ABDELWAHED, A. ELSABBAGH, M. A. TAHA: 'Experimental and numerical thermal monitoring of SS308L structures processed by wire arc additive manufacturing', *Prog. Addit. Manuf.*, (2025), https://doi.org/10.1007/s40964-025-01084-7.

[32] P. MEHMERT: *Numerische Simulation des Metallschutzgasschweißens von Grobblechen aus un- und niedriglegierten Feinkornbaustahl*, Dissertation, Clausthal, 2003.

[33] J. MÜLLER, J. HENSEL: 'Potential of thermography for the monitoring of DED-Arc processes', *Weld World*, 68 (2024), 505-513, https://doi.org/10.1007/s40194-023-01676-3.

[34] S. HARTMANN, O. MURUA, J. I. ARRIZUBIETA, A. LAMIKIZ, P. MAYR: 'Physics-informed neural network approach to speed up Laser-DED modelling', *Procedia CIRP*, 124 (2024), 352-357, https://doi.org/10.1016/j.procir.2024.08.132.

[35] B. PENG, A. PANESAR: 'Multi-layer thermal simulation using physics-informed neural network', *Additive Manufacturing*, 95 (2024), 104498, https://doi.org/10.1016/j.addma.2024.104498.

[36] G. MATTERA, L. NELE: 'Machine learning approaches for real-time process anomaly detection in wire arc additive manufacturing', *Int. J. Adv. Manuf. Technol.*, 137 (2025), 2863-2888, https://doi.org/10.1007/s00170-025-15327-y.